Numerical Study of the Aeroelastic Stability of an Overexpanded Rocket Nozzle

Emmanuel Lefrançois[*,**] **— Gouri Dhatt**[**] **— Dany Vandromme**[*]

[*] *LMFN CORIA UMR 6614*
INSA - Avenue de l'Université
BP08 76801 St Etienne du Rouvray, Cedex.

[**] *Université de Compiègne (UTC)*
Laboratoire de Roberval 60200 Compiègne, Cedex

emmanuel.lefrancois@utc.fr

ABSTRACT. A numerical model for studying aeroelastic stability is proposed in this paper with application to the overexpanded rocket engines. Starting from previous results obtained by Pekkari's team [PEK 93], the model is extended to take into account dynamic instabilities. A monodimensional model is used to check the effects of the chosen solicitation form on the global stability of a flexible nozzle. We observe that stability is influenced with the initial position of the separation shock. A static instability will be revealed by the presence of a zero value for one modal frequency, whereas a dynamic instability will appear after coalescing modes (similar to well-known flutter phenomena). Finally, a calculation is conducted in coupling two codes, one dedicated to structure dynamics, the second to the fluid phase in order to validate the stability model in the general two-dimensional case of an overexpanded rocket engine.

RÉSUMÉ. Nous présentons ici un modèle numérique de stabilité aéroélastique appliqué aux cas de divergents de moteurs fusée sur détendus (présence d'un choc de décollement). Partant du modèle développé par l'équipe de Pekkari [PEK 93], nous proposons une extension pour la prise en compte des instabilités de type dynamique. Après vérification sur un modèle 1D simplifié nous observons que la stabilité d'un divergent flexible, pour la forme de sollicitation analytique proposée par le modèle, est fonction de la position initiale du choc de décollement. La perte de stabilité statique apparaît suite à l'annulation d'une des fréquences fondamentales de la structure. Dans le cas dynamique, il s'agit d'une coalescence de deux fréquences, phénomène analogue au cas connu du flutter. Un calcul numérique avec couplage de codes, l'un dédié au fluide, l'autre à la structure, est finalement conduit pour permettre de valider la forme analytique de la sollicitation du modèle, dans le cas général d'une tuyère bidimensionnelle sur détendue.

KEY-WORDS: aeroelasticity, static and dynamic instabilities, rocket engines, separation shocks, coupled calculations, fluid-structure interaction.

MOTS-CLÉS: aéroélasticité, stabilités statique et dynamique, moteurs fusée, calculs couplés, chocs de décollement, interaction fluide-structure.

1. Introduction

During start-up and shut-down phases of a rocket engine, critical phenomena may appear and be responsible for damages or even an irreversible destruction of the divergent part of the nozzle.

During the starting phase of the engine, a first "blast" wave may sweep the whole nozzle to initiate the flow. Behind that first pressure discontinuity, the flow gets established by adjusting to the outside pressure ratio. That phase corresponds to the existence of a matching shock pattern, of which the longitudinal position is governed by the pressure field. That shock wave is attached to a complex flow separation in the nozzle. From the separation point, the nozzle jet encompasses periodic pressure structure known as pressure cells which may be found in any supersonic jet, with non-adapted pressure. The first cell structure inside the flow usually contains a Mach disk across the axis terminating at a triple point [SCH 84], [ROM 98]. There is no reason for this shock to evolve in a perfectly axisymmetric manner and then side loads effects may appear [SCH 73], [LEB 94], [NAV 73]. When appearing, they are detected before the complete stabilization of pressure chamber, the increase of which is progressive and effective after a few seconds according to the rocket engine. Side loads peaks are thus measured for particular values of the chamber pressure.

This phenomenon is known for a long time since the first works according to this, date back to the twenties, notably with Prandtl, Meyer and Stodola who worked on overexpanded jets [SUM 54]. In 1949, Forster and Cowles conducted measures on separated hot-gas flows [FOR 49]. The result of this work was that the separation condition corresponds to a pressure ratio of 40%. This ratio is often called the "Summerfield criterion" and is still in use today. In the mean time, the results of numerous cold-gas test and various hot-gas tests have been published which confirm the tendency of the measurements of Foster and Cowles.

The interest increased in the sixties when the same phenomenon was observed on the J2S engine of the Saturn V launcher [SCH 84]. From 1960 to 1966, NASA undertook a vast program of research to better understand the physics of side loads. It led to numerous theories and a huge amount of experimental data for side loads. However, the exact comprehension of the physics underlying such a phenomena is not totally clear and data correlations are complicated at best.

Today, this problem is still existing for rocket engines such as the SSME of the American space shuttle [REE 95], the Vulcain engine of the final version of Ariane V launcher [Pro98], [SER 96], [HAD 97] and other Japanese and Russian rocket engines. Recently, the solid rocket motor upgrade (SRMU) of Titan IVB launch vehicle dedicated to Cassini-Huygens mission on Saturn (satellites exploration), gave unexpectedly high nozzle actuator loads during ignition [ROM 98].

The main aspects susceptible to explain such phenomena are:

– Jet separation and its stability. This part is exclusively devoted to the study of fluid behaviour involving separation of the turbulent boundary layer, shock structure related to the main flow, influence of upstream disturbances or fluctuation in the downstream pressure field. This domain owns a rich bibliography and the interest evocated by many laboratories of the European community is well expressed in reference [Pro98];

– Aeroelasticity: This concerns the study of the mutual influence of the dynamical behaviour of a flexible structure on the flow.

In this paper, we focus on the aeroelasticity aspect to predict the structural behaviour of the nozzle rather than on an accurate study of the turbulence in separated flows.

Aeroelasticity has been studied for at least forty years from a theoretical point of view [DOW 75], [FUN 58], [BIS 75] and more recently a numerical approach has been developed and proposed [FAR 96], [KON 87], [TAL 96], [PIP 95b], [LEF 98]. The development of coupled models for aeroelasticity is quite recent due to its multidisciplinary nature. Moreover, its application to rocket engines has rarely been studied [TUO 68], [PEK 93]. It seems reasonable for this case to focus on the structural aspect, the engine being above all, the "organ" we wish to preserve.

The origin of the problem, when an aeroelastic phenomenon appears, is essentially due to the design of the rocket and the selected material for its construction. Indeed, the weight gain is the main concern in astronautics for which the objective is to launch the maximal payload for a given launcher weight, and thus for a given financial cost. The choice of a rigid and heavier material would probably resolve the problem but would have for main drawback to reduce accordingly the payload.
Thus, an efficient rocket structure is light in weight and thus quite flexible. The designer should carefully investigate the appearance of elastic instabilities, static buckling and flutter, to assure structural safety.

We may make the following remarks regarding the present state of rocket instability studies:

– Experimental data was published in 1968 by Tuovila [TUO 68] who detected an unstable behaviour similar to buckling on three of his five flexible nozzles. He recorded these results with a high-speed camera. His work is essentially rich in qualitative data;

– Experimental measures related to the response of actual rockets are almost nonexistent;

– Pekkari's team developed an aeroelastical stability model based on a simplification of the loads exerted by the separation shock on the nozzle leading to prediction of unstable modes [PEK 93].

The aim of this paper is to present certain aspects of a numerical model in order to offer a better understanding of aeroelasticity occurring in a rocket engine.

In this paper, we study the structural instabilities of a rocket type structure using simple aeroelastic models as well as fully coupled fluid-structure model. Our purpose is to assess the reliability of these models to predict unstable behaviour and to offer a better understanding of aeroelastic behaviour of the rocket structure.

In a first section, we start with a general presentation of a structural stability model under aerodynamic forces. This is followed by Pekkari's model involving a simplified representation of aerodynamic forces using "piston theory". We propose a linear dynamic instability model based on the finite element discretization to predict as well static as flutter behaviours. In a second part, results using eigenvalue analysis and direct time integration are exposed to better understand the flutter phenomenon. A coupled finite element fluid-structure model is then presented in the third section. It is based on *Parallel Virtual Machine* routines in order to establish a "message-passing" between two codes, one exclusively dedicated to fluid behaviour, the other for dynamical structure behaviour. In a fourth and last part, the latter coupled model is used to validate the stability model in conducting calculations on an overexpanded rocket engine with dimensions of class Vulcain.

2. Model for aeroelastical stability

In this section, we present a general dynamic stability model leading to Pekkari's model and an extended finite element model.

2.1. *Dynamic stability*

Set a structure in equilibrium for a given configuration C_o be subjected to a perturbation load. The dynamic equilibrium is defined by:

$$m\ddot{\vec{w}} = \vec{f}_m^o(w_o) + \vec{f}_a^o(w_o) + \vec{f}_m(w) + \vec{f}_a(w), \qquad [1]$$

where m is the local mass of the system, $\vec{f}_m^o(w_o) + \vec{f}_m(w)$ and $\vec{f}_a^o(w_o) + \vec{f}_a(w)$ are respectively the internal and aerodynamic forces. Each of them is composed of an equilibrium part indiced by "o" and a perturbated part. The terms $\vec{f}_m(w)$ and $\vec{f}_a(w)$ express all modifications of the equilibrium case. The terms w and $\ddot{w}$ are respectively the local displacement of the structure in response to external disturbances and corresponding perturbated acceleration. For the particular case of equilibrium, we have then:

$$\vec{f}_m^o + \vec{f}_a^o = 0.$$

A finite element discretization of the Equation [1] gives:

$$[M]\{\ddot{W}\} + [K]\{W\} = \{F(W)\}, \qquad [2]$$

where $[M]$ and $[K]$ are respectively the mass and stiffness matrices, $\{W\}$ the global displacement vector on each node of the structure mesh, $\{\ddot{W}\}$ the corresponding acceleration and $\{F\}$ the global forces vector resulting from the aerodynamic coupling.

The aerodynamic force vector $\{F(W)\}$ may be written in the following form:

$$\{F\} = [K^*]\{W\},$$

where $[K^*]$ is an unsymmetrical matrix.

Equation [2] then becomes:

$$[M]\{\ddot{W}\} + ([K] - [K^*])\{W\} = \{0\}. \qquad [3]$$

The stability of Equation [3] may be obtained by analyzing its natural frequencies. For a linear system with regards to $[M]$, $[K]$ and $[K^*]$, we may represent the solution under the following decomposition form:

$$\{W(x_i, t)\} = \{\bar{W}(x_i)\}e^{i\Omega t}, \quad \Omega : \text{natural frequency},$$

it leads to the following free vibration model:

$$\left(([K] - [K^*]) - \Omega^2[M]\right)\{\bar{W}\} = \{0\}. \qquad [4]$$

For given matrices $[M]$ and $[K]$, the stability of the system is governed by the aerodynamic matrix $[K^*]$ which depends on the intensity of the aerodynamic load.

The system is statically unstable for $[K^*]$ such as it leads to $\Omega = 0$ and then:

$$([K] - [K^*])\{\bar{W}\} = \{0\}.$$

The system is dynamically unstable if $[K^*]$ leads to complex conjugate values of Ω such as:

$$\left(([K] - [K^*]) - \Omega^2[M]\right)\{\bar{W}\} = \{0\}, \quad \text{with} \quad \Omega = a \pm ib. \qquad [5]$$

The appearance of flutter is thus related to coalescing between two frequencies with the appearance of negative damping (imaginary part b of Ω).

If one obtains the eigen-space using:

$$[K]\{X_i\} = \omega^2[M]\{X_i\},$$

Equation [4] expressed in the modal space $\{X_i\}$ becomes:

$$\left(\Omega^2 \begin{bmatrix} 1 & & 0 \\ & \ddots & \\ 0 & & 1 \end{bmatrix} - \left(\begin{bmatrix} \omega_1^2 & & 0 \\ & \ddots & \\ 0 & & \omega_n^2 \end{bmatrix} - [\bar{K}^*] \right) \right)\{v\} = \{0\}, \qquad [6]$$

with:

$$\{W\} = [X]\{v\}; \quad [\bar{K}^*] = [X]^T[K^*][X].$$

The matrix $[X]$ corresponds here to the set of the eigenvectors $\{X_i\}$.

A simplified version of frequency modification of ω_i by aerodynamic coupling is obtained from Equation [6]:

$$\Omega_i^2 = \omega_i^2 - \bar{K}_{ii}^*, \qquad [7]$$

where only the diagonal terms of $[\bar{K}^*]$ have been retained. With this assumption, it is thus possible to estimate only static instability. Such a model cannot represent flutter instability for reasons we will explain later.

2.2. *Application to a rocket engine: Problem overview*

We are interested in studying the global stability of a Laval nozzle (supersonic convergent-divergent). A representation is given in Figure 1:

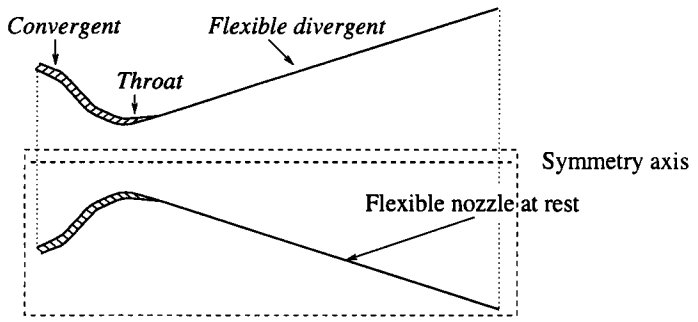

Figure 1. *Laval nozzle configuration*

What follows is based on the approach proposed by Pekkari [PEK 93] to study the aeroelastical stability on a rocket engine. This is described as follows:

– A Laval nozzle in an initial steady state configuration (Figure 1) is subject to an overexpanded flow condition. A separation shock develops and finally stabilizes (Figure 2) accordingly with a modified structure state,

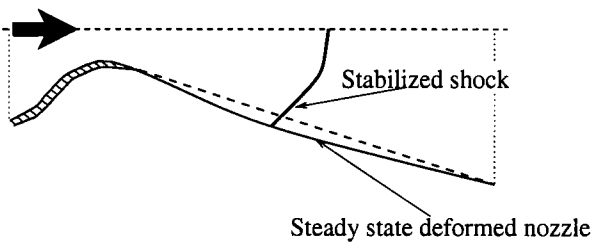

Figure 2. *Half nozzle in equilibrium with pressure forces*

– Simultaneous changes on the shock location and the nozzle wall geometry may lead to a fluid-structural coupling (Figure 3) .

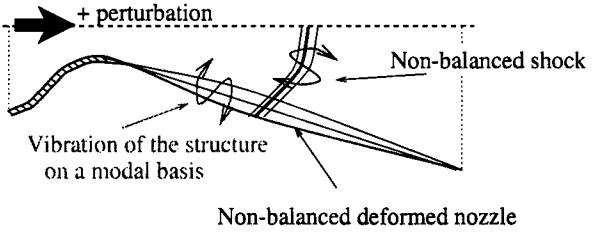

Figure 3. *Fluid-structure coupling for a non-equilibrium state*

For the case where wall displacements are "small" enough for a linear theory to apply, the time evolution of the global structure may be considered as a linear combination of modal deformations associated to particular frequencies, deformations that may be not necessarily equal to the natural ones.

We propose to study the influence of the initial position of the separation point (location of the compression shock) on the overall global stability of the flexible nozzle.

2.2.1. *Hypotheses*

The hypotheses are as follows:

– The system is considered as quasi-steady with respect to the flow because time scales between the fluid and the structure are distinct from several orders of magnitude: $\Delta t_{fluide} << \Delta t_{structure}$.
It permits to simplify the fluid flow model by neglecting the inertial effects;

– The geometry is two-dimensional with a unit width;

– The fluid is assumed perfect, compressible and inviscid. The pressure profile $p_\infty(x)$ along the nozzle is obtained using analytical relations for isentropic flow with sections: for given section profile $A(x)$ and chamber conditions in pressure and temperature (respectively P_c and T_c), it is then possible to calculate static pressure $p_\infty(x)$ and Mach number $M_\infty(x)$ as functions of the section $A(x)$ with analytical relations [CAN 90].
From this analytical pressure profile, a normal shock is considered at location x_{sep} by using a separation criteria such as Schmucker criteria [SCH 84].
The global wall pressure is thus defined by:

$$p(x) = \begin{cases} p_\infty(x) + \dfrac{\rho_\infty U_\infty^2}{\sqrt{M_\infty^2 - 1}} \dfrac{\partial w_n}{\partial s} + ..., & x < x_{sep}, \\ p(x_{sep}) = p_{sep}, \text{ such as } \dfrac{p_{sep}}{p_a} = 0.3, 0.4, ... & x = x_{sep}, \\ p_a, & x > x_{sep}, \end{cases} \quad [8]$$

where $p_\infty(x)$ is the static pressure resulting from the flow expansion and p_a the external pressure. The variables ρ_∞, U_∞ and M_∞ are respectively the density, the streamwise velocity and the Mach number of the fluid where the static pressure is equal to $p_\infty(x)$.
The second term in the first equation in [8] is based on a simplified form of the piston theory [ASH 56], where w_n represents the normal displacement of the wall.
Beyond the separation point located at x_{sep}, the pressure is taken equal to the ambient pressure p_a.
Eventually, the pressure in the area covered by the separation point is taken to p_{sep}, x^o_{sep} being the initial position of the separation shock;

– The stressed structure being initially in equilibrium (Figure 2), the solicitation term will be calculated from the forces resulting from the motion of the separation point between the initial and current positions [PEK 93]:

$$\vec{f}_a(x,w) = \vec{n}(p_a - p_{sep})(I\!H[x - x_{sep}] - I\!H[x - x^o_{sep}]), \qquad [9]$$

where $I\!H$ function acts as a filter given by the following law:

$$I\!H[z] = \begin{cases} 0, & \text{if } z < 0, \\ 1, & \text{if } z \geq 0. \end{cases}$$

It permits to consider a non-zero solicitation term on the area covered by the shock and equal to zero elsewhere, such as:

$$\int_{x^o_{sep}}^{x_{sep}} \vec{f}_a ds = \vec{n}(p_a - p_{sep})(x_{sep} - x^o_{sep}).$$

Introducing the first order expansion around x^o_{sep} of $p_\infty(x)$ in the relation [8], it leads to:

$$p(x) \approx p_\infty(x^o_{sep}) + (x - x^o_{sep}) \left(\frac{dp_\infty}{dx}\right)_{x^o_{sep}} + \frac{\rho_\infty U_\infty^2}{\sqrt{M_\infty^2 - 1}} \left.\frac{\partial w_n}{\partial s}\right|_{x^o_{sep}} + \ldots$$

For $x = x_{sep}$, this finally leads to the relation:

$$x_{sep} - x^o_{sep} = \frac{\rho_\infty U_\infty^2}{\left(\frac{dp_\infty}{dx}\right)_{x^o_{sep}} \sqrt{M_\infty^2 - 1}} \left.\frac{\partial w_n}{\partial s}\right|_{x^o_{sep}},$$

by assuming that: $p(x_{sep}) \approx p_\infty(x^o_{sep}) \approx p_{sep}$.

By using this previous expression, we finally obtain the aerodynamic matrix $[K^*]$:

$$<\delta W>[K^*]\{W\} = <\delta W>\{F\} = \int_{x^o_{sep}}^{x_{sep}} \delta\vec{w}.\vec{n}(p_a - p_{sep})dS,$$

$$\approx <\delta W>\ (p_a - p_{sep}) \frac{\rho_\infty U_\infty^2}{-\left(\frac{dp_\infty}{dx}\right)_J \sqrt{M_\infty^2 - 1}} \begin{pmatrix} n_x \\ n_y \\ 0 \end{pmatrix}_J \left.\frac{\partial W_n}{\partial s}\right|_J, \qquad [10]$$

where J denotes the nodal indice corresponding to the separation point and $< \delta W >$ is the nodal test function vector used in a finite element approach.

2.2.2. *Aeroelastic stability model*

The purpose of the stability analysis is to verify if the structure is stable for:

– A given flow situation i.e. $\rho_\infty(x)$, $M_\infty(x)$, U_∞;

– Pressure distribution parameters: $p_\infty(x)$; $\dfrac{p_a}{p_{sep}}$ and $\dfrac{dp_\infty}{dx}$;

– An initial separation shock position at x^o_{sep} .

The Pekkari's model is based on Equation [6]. We recall that this latter has been obtained after having applied a projection of the global solution on the eigenmodal vectors base $[X]$, such as: $\{W\} = [X]\{v\}$.

If we only retain the diagonal terms of the perturbated matrix $[K^*]$ in Equation [6], it leads to the expression [7] given in [PEK 93]:

$$\Omega_k^2 = \omega_k^2 - (p_a - p_{sep}) \frac{\rho_\infty U_\infty^2}{\left(-\frac{dp_\infty}{dx}\right)_J \sqrt{M_\infty^2 - 1}} X_n^k\big|_J \left.\frac{\partial X_n^k}{\partial s}\right|_J , \qquad [11]$$

where Ω_k and ω_k are respectively the forced and the natural pulsation associated to the k^{th} mode of the structure.

The term $X_n^k\big|_J$ denotes the normal displacement at J node of the k^{th} natural mode. We deduce from the previous equation that according to the second term amplitude in the right part of the equation, Ω_k^2 may become null and thus express a static instability such as buckling.

However, only statical instabilities may be deduced form this equation. Dynamical ones appear by coalescing between two modes associated to two complex conjugate eigenfrequencies. It thus requires:

– Complete form of the unsymmetrical matrix $[K^*]$ to allow eigenfrequencies becoming complex and conjugate;

– Coalescing effect between two eigenfrequencies also affects the corresponding eigenvectors. This point explains why the Pekkari's model is unable to predict such a phenomenon because of the projection of the solution on a constant eigenvectors base $[X]$. Moreover, there is no particular reason that coalescing eigenvectors be a linear combination of natural ones.

2.2.3. *Finite element analysis model*

Based on the general instability model [5] and the expression of $[K^*]$ given by [10], we propose the following approach to study the stability for the most general

case (static and dynamic):

– For a given initial shock position x^o_{sep}, corresponding to a particular chamber pressure value P_c and a given separation criteria $\frac{p_a}{p_{sep}}$:

- Identify the flow parameters: $\rho_\infty(x)$, $M_\infty(x)$, ...;
- Identify the pressure parameters: $p_\infty(x)$, $\frac{dp_\infty}{dx}$;
- Calculate the corresponding aerodynamic matrix $[K^*]$ by Equation [10];
- Obtain the eigenvalues Ω_i^2 of [5] by modal analysis.

– Choose next shock position according to a new chamber pressure value.

We propose in the next section to determine the evolution of the natural frequencies in regards with the shock position for a given nozzle configuration. Three different calculations will be conducted with:

– Pekkari's simplified model based on Equation [11];

– Extended model for flutter analysis with [5];

– Direct time integration in using expression [10] for the solicitation term.

2.3. *"Analytical" validation of the stability model*

The previous model can be tested by directly introducing the solicitation term given by the Equation [10] in a structural analysis code. The objective is to verify the instabilities predicted by the model for given material properties.

The structure code is based on a finite element method. It solves the system [2] in using a Newmark scheme for the time discretization. The only modification consists in directly applying the solicitation [10] after extracting nodal displacements of the previous time step.

The domain of calculation is illustrated on Figure 4:

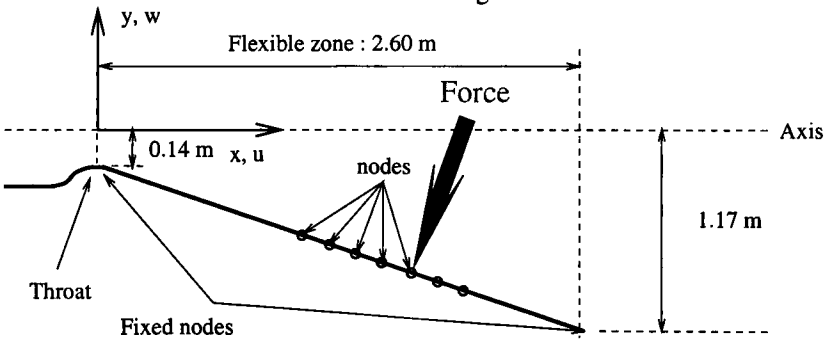

Figure 4. *Model for flexible nozzle*

It consists on a two-dimensional geometry whose the dimensions correspond to a Vulcain class engine. However, in order to reduce two-dimensional effects, the profile of the nozzle has been chosen straight instead of parabolic. Only the divergent part is supposed flexible and is meshed using two-nodes beam elements. The mesh is made of 40 uniformly distributed nodes.

The material properties of the structure are as follows:

Young modulus	Thickness	Poisson coefficient	Mass density
$2.2\ 10^{11}\ N/m^2$	$1\ 10^{-2}\ m$	0.0	$2000\ kg/m^3$

Concerning the fluid properties and characteristics, we have:

Range for P_c [bar]	T_c [K]	Range for shock position [m]	p_a/p_{sep}	p_a [bar]
$[0.5\ -\ 6.5]$	2400	$[0.1\ -\ 2.55]$	15.5	10^5

The value given to the separation criteria (p_a/p_{sep}) has been obtained from previous two-dimensional fluid calculations on the same domain. One may also show that stability results are very little dependent on the value given to this separation criteria.

The results obtained from the direct calculation of the Equation [11] (after a previous modal analysis for obtaining $[X]$) are presented in dashed lines on Figure 5. The results obtained from the resolution of [5] for each nodes corresponding to an initial shock position, are also presented on Figure 5 in continuous lines.

We can make the following observations:

– For an initial position surrounding $x_{sep} \approx 0.8$ the first natural mode collapses with the zero-axis expressing a buckling effect. This behaviour is also reported in using the Pekkari's model;

– For x_{sep} belonging to the range $[1.4\ -\ 1.8]$, the first two natural modes collapse in complex conjugate eigenfrequencies. This expresses a dynamical instability similar to *flutter*. This case is not observed with Pekkari's model for which all frequencies remain real. It is due to the fact that for this model, eigenvectors used for modal projection are supposed unchanged and prevent this instability to appear. However, both models remain close of the global trend.

REMARQUE.— *For a smaller Young modulus (results not shown here) that strengthens the collapsing modes effect, we observe for the Pekkari's model that the first two natural modes pass each other with no mutual interaction as a swapping-modes.*

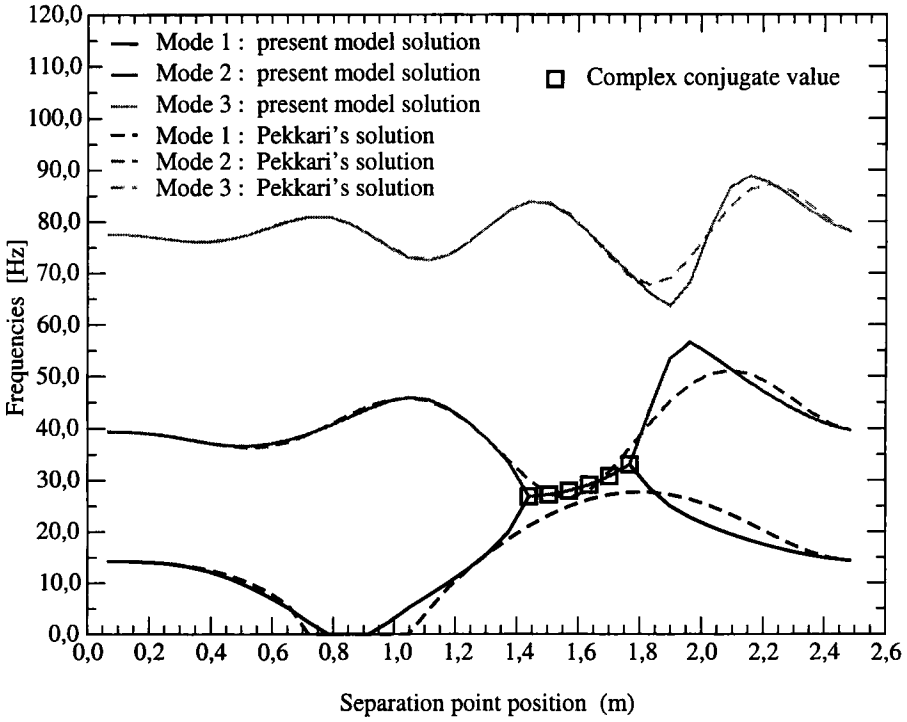

Figure 5. *Analytical profiles for the first three modes*

For the third calculation that corresponds to an the analytical validation of this model, a first step consists in introducing the solicitation form [10] in a structure code dedicated to dynamical simulation. The calculation has been conducted in applying the solicitation on several nodes to obtain the results presented on Figures 6, 7 and 8.

For each case, we represent on the upper graph the temporal evolution of the radial displacement taken at the considered point. The lower graph is the spectrum of the previous signal obtained from a "Fast Fourier Transform" procedure. The time step has been taken equal to $\Delta t_s = 1.10^{-4}$s and 2000 steps have been conducted.

These results show the frequencies deviation forecasted by the stability model and confirm the coalescing effect between the first two modes and its exponential growing typical of the dynamical instabilities for the case $x_{sep} = 1.54\ m$.

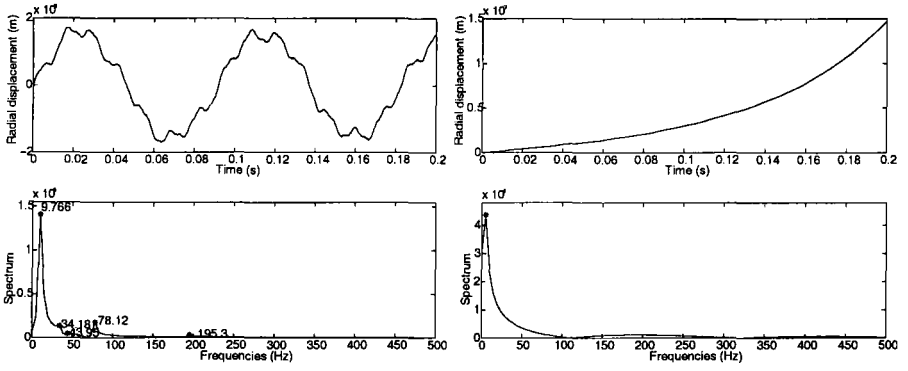

Figure 6. *Results for* $x_{sep} = 0.45\ m$ - *Results for* $x_{sep} = 0.85\ m$

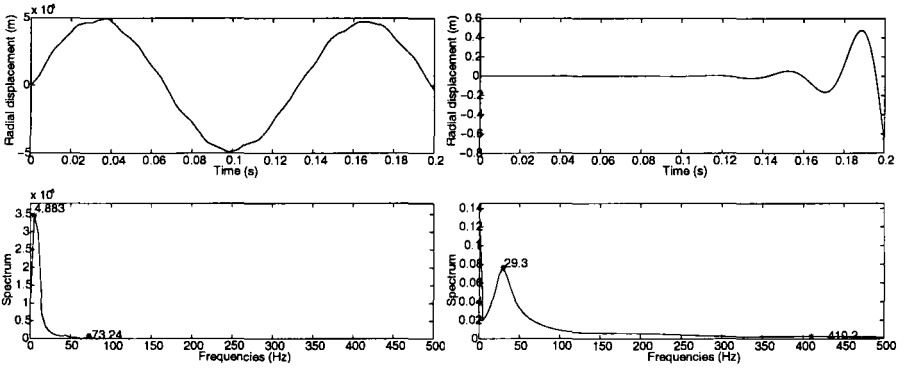

Figure 7. *Results for* $x_{sep} = 1.10\ m$ - *Results for* $x_{sep} = 1.54\ m$

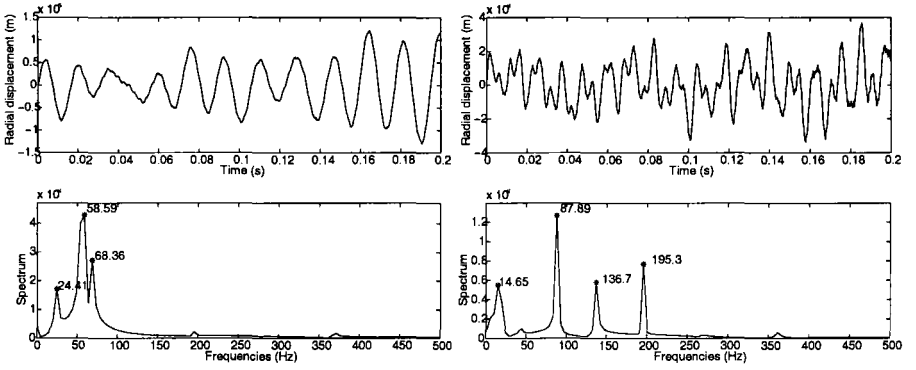

Figure 8. *Results for* $x_{sep} = 1.94\ m$ - *Results for* $x_{sep} = 2.20\ m$

However, these results do not constitute a complete validation because of the introduction of the particular form of the solicitation. In the following sections we will attach ourselves to validate the stability model in a more objective way in taking two different codes respectively dedicated for fluid and structure calculations and letting them proceed to their own coupling.

3. Numerical model for fluid-structure calculations

The coupling model considered in this section has been previously developed in [LEF 98], [LEF 99c] and [LEF 99b].

It consists of two numerical codes, one exclusively dedicated to fluid calculations, the other for structural dynamics.

Here, we briefly expose characteristics of both codes:

– Structure code:

- A *Total Lagrangian Formulation* is employed to calculate the deformations of a flexible structure under large displacements hypothesis [DHA 95a];

- The resolution of the resulting non-linear system is obtained using a Newton-Raphson iterative method [DHA 95c], [AMM 96];

- Two finite elements are proposed in geometrical non-linearities assumptions, a two-dimensional two-nodes beam element and an axisymmetrical shell element [LEF 99c], [LEF 99b], [DHA 95b];

- An implicit Newmark scheme is used for temporal resolution of dynamical terms.

– Fluid code:

- The fluid is supposed compressible and inviscid and the flow is considered two-dimensional or axisymmetric;

- An explicit Lax-Wendroff scheme is used for temporal discretization [LAX 60] with a shock capturing technique called *Flux Corrected Transport* [BOR 97] in zones where positivity is not ensured (shocks);

- In order to ensure geometrical compatibility between both fluid and structure meshes, and to avoid excessive mesh distortion, a dynamic mesh technique is used to totally adapt fluid mesh to wall deformation. A geometrical consistency law is applied to the dynamic mesh in order to ensure independency of the fluid variables in regard with the mesh motion [FAR 96], [LEF 99c];

- Stability is ensured using a CFL criteria [COR 92].

– Coupling:

- In order to preserve modularity aspects of each code taken separately, the coupling is done in establishing a "message-passing" between solvers by using parallel tools offered by PVM (*Parallel Virtual Machine*) routines [GEI 94], [KES 97];

- The exchanged data during calculations consist of the wall pressure distribution and time step from the fluid code to the structure one, and the update of the flexible boundaries common to both codes from the structure to the fluid;

- The characteristic times being different by several orders of magnitude between both codes (implicit structure code and explicit fluid code), the updating of wall conditions is made using a subcycling coupling scheme and thus carried out every $N_{f/s}$ fluid steps;

- Several subcycling schemes may be employed depending on the required accuracy (with CPU considerations) and the type of common wall boundary at the interface. Usually, kinematic compatibility and energy conservation are not both ensured simultaneously.

3.1. *Structure model*

The variational form of the equilibrium relations may be written as follows:

$$W = \int_{V(t)} \delta\vec{u}\rho\frac{d^2\vec{u}}{dt^2}dV + \int_{V(t)} \vec{\nabla}\delta\vec{u} : \sigma dV - \int_{V(t)} \delta\vec{u}\vec{f}_v dV - \int_{S(t)} \delta\vec{u}\vec{f}_s dS = 0,$$

with σ the Cauchy's stress tensor, $\vec{f}_s$ and $\vec{f}_v$ the external solicitations respectively surfacic and volumetric, $\vec{\delta u}$ a test function and $\vec{u}$ the displacements vector.

In the case where small perturbations hypothesis is not verified any more, a Total Lagrangian Formulation [DHA 95a] is used to express the weak form on the current configuration $V(t)$ and $S(t)$:

$$W = \int_{V^o} \delta\vec{u}\rho_o\frac{d^2\vec{u}}{dt^2}dV^o + \int_{V^o} \delta\mathcal{E}_{gl} : SdV^o - \int_{V^o} \delta\vec{u}\vec{f}_{vo}dV^o - \int_{S^o} \delta\vec{u}\vec{f}_{so}dS^o = 0, \quad [12]$$

where:

- ρ_o: density on (V^o, S^o) configuration,
- $\delta\vec{u}$: test function,
- $\delta\mathcal{E}_{gl}$: variation of Green-Lagrange deformation tensor,
- $\vec{f}_{so}$, $\vec{f}_{vo}$: external solicitations on C^o,
- S: Piola-Kirchhoff stress tensor (2^{nd} species).

The Green-Lagrange deformation tensor is determined in the general way:

$$\mathcal{E}_{gl} = \frac{1}{2}\left(F^T F - I\right), \quad \text{where} \quad \mathcal{F} = \frac{\partial\vec{x}}{\partial\vec{x}^o}, \quad [13]$$

with $\mathcal{F}$ the transformation gradient tensor and I the unity tensor.

The stress and deformation tensors are related using a linear elastic behaviour:

$$S = \mathbb{H}\mathcal{E}_{gl},$$

with $\mathbb{H}$ the property matrix.

A finite element technique is used for space discretization. It leads to the non-linear system:

$$[M]\left\{\frac{\partial^2 u}{\partial t^2}\right\} + \{f_{int}(u,t)\} - \{f_{ext}\} = 0, \qquad [14]$$

obtained after assembling all over the mesh elements where:

- $[M]$: global mass matrix,
- $\{u\}$: nodal displacements vector,
- $\{f_{int}(u,t)\}$: non-linear internal efforts,
- $\{f_{ext}\}$: external forces resulting from aerodynamical coupling.

The element used in this paper is a 2-nodes beam that will not be presented here. We invite interested readers to consult the references [LEF 98], [LEF 99c].

A Newmark scheme is then used for the temporal discretization. An iterative Newton-Raphson is used to solve the non-linear system given by [14]. It means the calculation of a tangent matrix given by the variation of the weak form [12] and obtained as follows:

$$\Delta W = \int_{V^o} \delta\vec{u}\rho_o \frac{d^2\Delta\vec{u}}{dt^2} dV^o + \int_{V^o} (\delta(\Delta\mathcal{E}_{gl}) : \mathcal{S} + \delta\mathcal{E}_{gl} : \Delta S)\, dV^o. \qquad [15]$$

After each time step, the geometry is updated, the deformations and strains are all calculated from initial configuration with regards to the Total Lagrangian formalism.

3.2. *Fluid model*

The conservation laws for conservative quantities of compressible and inviscid flow on a two-dimensional moving domain may be written as [FAR 96], [LEF 99c]:

$$\frac{\partial}{\partial t}\{JU\} + J\left(\frac{\partial\{F_x\}}{\partial x} + \frac{\partial\{F_y\}}{\partial y}\right) = 0, \qquad [16]$$

where:

- $\{U\}$: conservative variables,
- $\{F_x\} = \{F_{cx}\} - w_x\{U\}$: convective flux along x-direction,
- $\{F_y\} = \{F_{cy}\} - w_y\{U\}$: convective flux along y-direction,

with:

$$\{U\} = \begin{pmatrix} \rho \\ \rho u \\ \rho v \\ \rho e \end{pmatrix}, \quad \{F_{cx}\} = \begin{pmatrix} \rho u \\ \rho u^2 + p \\ \rho uv \\ (\rho e + p)u \end{pmatrix}, \quad \{F_{cy}\} = \begin{pmatrix} \rho v \\ \rho uv \\ \rho v^2 + p \\ (\rho e + p)v \end{pmatrix},$$

with ρ the mass density, u and v respectively the components of fluid velocity in (x, y) system, e the total energy per unit of mass and p the local pressure given by the law of perfect gas:

$$p = \rho.r.T = (\gamma - 1)(\rho e - 1/2\rho(u^2 + v^2)),$$

with the temperature T, $\gamma = 1.4$ and $r = 287u.SI$.
The variables (w_x, w_y) represent the local velocity components of the domain.

One may obtain a weak form by integrating by parts:

$$W_f = \frac{\partial}{\partial t}\int_{V(t)} < \delta U > \{U\}dV - \int_{V(t)} (< \delta U_{,x} > \{F_x\} + < \delta U_{,y} > \{F_y\})\, dV + \oint_{S(t)} < \delta U > (\{F_x\}n_x + \{F_y\}n_y)\, dS = 0, \qquad [17]$$

where $< \delta U >$ is a test function on the reference space and where (n_x, n_y) are the components of the external normal vector at the boundary.

3.2.1. *Geometrical consistency*

We suppose that mesh displacement within the interval $(t, t + \Delta t)$ is defined as follows:

$$\vec{X_f}(\tau) = (1 - \phi(\tau))\vec{X_f}^{\,p}(\xi, \eta) + \phi(\tau)\vec{X_f}^{\,p+1}(\xi, \eta),$$

leading to:

$$\vec{w}(\xi, \eta) = \dot{\phi}(\vec{X_f}^{\,p+1} - \vec{X_f}^{\,p}),$$

with $\phi(\tau = t) = 0$ and $\phi(\tau = t + \Delta t) = 1$ and (ξ, η) are reference coordinates for a two-dimensional model.
The Jacobian matrix is obtained in a general way:

$$[J]^T = [F(\tau)] = \left[\frac{\partial \vec{X_f}}{\partial \xi} \quad \frac{\partial \vec{X_f}}{\partial \eta}\right] = ((1 - \phi(\tau))[F]^p + \phi(\tau)[F]^{p+1},$$

and the determinant is quadratic in ϕ for two-dimensional cases:

$$J(\tau) = det(F(\tau)) = a_0 + a_1\phi(\tau) + a_2\phi^2(\tau) \qquad [18]$$

For a fixed mesh, the Lax-Wendroff finite element model satisfies the consistency and stability conditions (see [BOU 93]). For a moving mesh, it is essential that uniform flow field be exactly conserved (according to the so-called geometrical consistency

law) for any moving mesh. If we consider a uniform flow that corresponds to constant $\{U\}$, the Equation [16] becomes for each component of $\{U\}$:

$$\frac{\partial J}{\partial t} - J.Div\vec{w} = 0. \qquad [19]$$

In weak form, we have:

$$\frac{\partial}{\partial t}\int_V \psi dV = \int_V \psi Div\vec{w} dV,$$

where ψ is a test function representing each component of $\{\delta U\}$. For geometrical consistency, it is then essential this relation be exactly satisfied by the discrete model. The time integration leads to:

$$\begin{aligned}
\int_{V^{p+1}} \psi dV - \int_{V^p} \psi dV &= \int_t^{t+\Delta t}\int_{V_\tau} \psi J Div\vec{w}\, dV_\tau d\tau \\
&= \int_t^{t+\Delta t}\int_{V_\tau} \psi \frac{\partial J}{\partial \tau} dV_\tau d\tau \text{ using [19]} \\
&= \int_t^{t+\Delta t}\int_{V_\tau} \psi(a_1\dot{\phi}(\tau) + 2a_2\phi(\tau)\dot{\phi}(\tau)) dV_\tau d\tau \text{ using [18]} \\
&= \int_0^1\int_{V_\tau} \psi(a_1 + a_2\phi(\tau)) dV_\tau d\phi. \qquad [20]
\end{aligned}$$

The right term in the last equation is linear in $\phi(\tau)$. The space integration is guaranteed by standard finite element integration. Since the variation is linear in $\phi(\tau)$, the midpoint rule integration is sufficient to integrate exactly this last term. In our case, $\phi(\tau)$ has been chosen linear in τ and then the integration point corresponds to $\phi(\tau = \frac{1}{2}) = \frac{1}{2}$.
Recalling that we are interested in integrating $Div\vec{w}$, it leads to:

$$\int_{V^{p+1}} \psi dV - \int_{V^p} \psi dV = \Delta t \int_{V^{p+1/2}} \psi Div\vec{w} dV,$$

that corresponds to an integration over the domain located at $p + 1/2$ and defined by

$$\vec{X_f}^{p+1/2} = \frac{\vec{X_f}^{p+1} + \vec{X_f}^{p}}{2}.$$

The corresponding mesh field velocity is calculated as follows:

$$\vec{w}^{p+1/2} = \dot{\vec{X}}_f = \frac{\vec{X_f}^{p+1} - \vec{X_f}^{p}}{\Delta t}.$$

After discretization of the weak form [17] and applying the previous midpoint integration rule, it leads to the system:

$$[M]^{p+1}\{U\}^{p+1} - [M]^p\{U\}^p = \{R\}^{p+1/2},$$

that can be written in an incremental way:

$$[M]^{p+1}\{\Delta U\} = \{R\}^{p+1/2} + \left([M]^p - [M]^{p+1}\right)\{U\}^p = \{\mathcal{R}\}, \qquad [21]$$

where:

- $[M]^p$, $[M]^{p+1}$: global mass matrix at instants t and $t + \Delta t$;
- $\{\Delta U\} = \{U\}^{p+1} - \{U\}^p$: incremental solution;
- $\{R\}^{p+1/2}$: global residual vector obtained from $\{U\}^{p+1/2}$;
- $\{\mathcal{R}\}$: modified residual vector due to $[M]^p$ and $[M]^{p+1}$.

To solve [21], we perform about 2 or 3 Jacobi iterations using diagonalized preconditioned mass matrix (good condition number). Thus, the solution process becomes very efficient.

A linear triangular element is used for space discretization and we invite interested readers to consult references given in [LEF 98], [LEF 99c] for the finite element description and additive informations.

In high gradient zones, the non-positive nature of Lax-Wendroff [LAX 60] scheme may produce spurious oscillations. The idea behind stabilization techniques (Flux Corrected Transport in our case [PAR 85]) is to consider a first order scheme in high gradient zone and to conserve higher order Lax-Wendroff scheme elsewhere.

Inflow and outflow boundary conditions are solved using characteristics theory [COR 92]. A slip condition is imposed on solid wall boundaries and symmetric axis. For moving wall boundaries, the normal fluid velocity is imposed equal to the normal component of the wall velocity.

The mesh velocities are obtained using linear interpolation in both direction as shown on Figure 9:

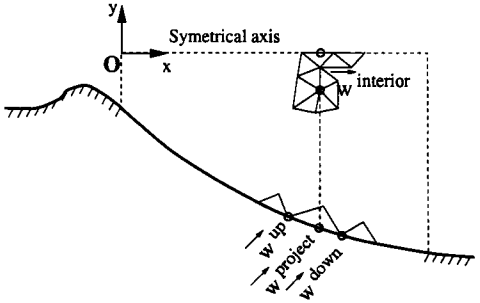

Figure 9. *Mesh adaptation*

– For each interior moving node, locate its radial projection on flexible boundary and search the two neighboring nodes whose velocities are known, $\vec{w}^{up}$ and $\vec{w}^{down}$;

– Calculate $\vec{w}^{project}$ of projected point by using linear interpolation between $\vec{w}^{up}$ and $\vec{w}^{down}$;

– Obtain interior node velocity by linear interpolation between $\vec{w}^{project}$ and zero-velocity on symmetrical axis.

3.3. *Continuous coupling scheme*

A coupling scheme is a list of operations to execute in a given order between two codes in order to permit the message-passing of common data.

A complete cycle takes place as follows:

– The fluid transmits to the structure the pressure profile obtained at time (n);

– The structure code determines the displacements solution (X^{n+1}, Y^{n+1}) at instant $(n+1)$ obtained from pressure data corresponding to instant (n);

– This structure configuration is transmitted to the fluid code i.e. displacements and velocities of all nodes denoted by (X^{n+1}, Y^{n+1}) and $(\dot{X}^{n+1}, \dot{Y}^{n+1})$;

– Fluid variables are then advanced of $N_{f/s}$ fluid time steps in order to reach the new structure deformation;

– Back to step 1.

The boundary conditions are:

$$\begin{aligned} X_{fluid}(t) &= X_{structure}(t) \ \ \forall t \ \text{ at the interface,} \\ \dot{X}_{fluid}(t) &= \dot{X}_{structure}(t) \ \ \forall t \ \text{ at the interface.} \end{aligned} \qquad [22]$$

The geometric consistency law imposes a mesh velocity given by:

$$\dot{X}_f^{n+1/2} = \frac{X_f^{n+1} - X_f^n}{\Delta t_s}, \qquad [23]$$

where X_f^{n+1} and X_f^n denote the fluid mesh states respectively at times (n) and $(n+1)$. This choice must be compatible with the Newmark temporal discretization scheme used in the structure solver. Thus, we may show that if the fluid mesh velocity must be constant between two fluid time steps, it must be re-calculated after each fluid time step. This is due to the Newmark scheme that considers a constant average acceleration between two structure steps leading thus to a linear evolution of the velocity field

over the $N_{f/s}$ fluid time steps. This is illustrated on Figure 10:

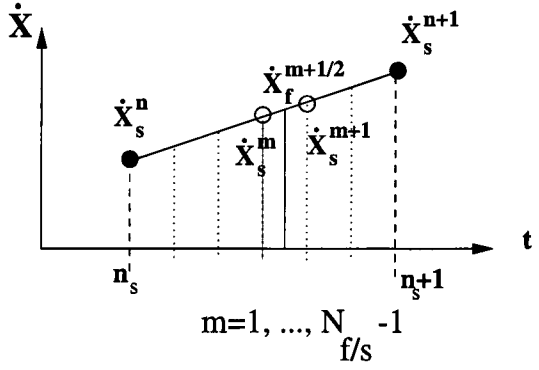

Figure 10. *Compatibility between fluid and structure velocities*

We may prove [PIP 95a] that the total energy exchanges between fluid and structure between two successive updates of the structure is given by:

$$\begin{aligned} E^{n+1} \quad & -E^n = \Delta E_f + \Delta E_s \\ = \quad & \sum_{ie=1}^{nelt} \left[\frac{1}{N_{f/s}} \sum_{ip=1}^{N_{f/s}} \underbrace{\bar{P}_{ie,ip}}_{\text{Fluid}} - \underbrace{P_{ie}^*}_{\text{Structure}} \right] \left((X^{n+1}-X^n) n_x + (Y^{n+1}-Y^n) n_y \right) \\ \neq \quad & 0, \end{aligned}$$

where $\bar{P}_{ie,ip}$ corresponds to the average pressure on the ie^{th} element at fluid time step (ip), L is the element length, $nelt$ the total number of elements and (n_x, n_y) the normal vector components. The term P_{ie}^* corresponds to the pressure value transmitted by the fluid code to the structure one and constant during the $N_{f/s}$ fluid time step.

We observe for this case that the energy conservation is not ensured and is proportional to the difference between two successive structure states. Previous studies [LEF 99a] on the flutter test-case has shown that for $N_{f/s} > 5$, results may become inaccurate!

Moreover, we may prove that action-reaction principle is not even more ensured between fluid and structure where the sum of each one that should collapse to zero is effectively given by:

$$\text{Force (Fl. -> St.)} = -\Delta t_s \bar{P}_{ie}, \quad \text{Force (St. -> Fl.)} = \frac{\Delta t_s}{N_{f/s}} \sum_{ip=1}^{N_{f/s}} \bar{P}_{ie,ip}, \qquad [24]$$

and then:

$$\Rightarrow \text{Force (Fl. -> St.)} + \text{Force (St. -> Fl.)} \neq 0 \ !$$

This is the reason why this scheme will not be used for this study and we will prefer the discontinuous scheme exposed on the next section.

3.4. *Discontinuous coupling scheme*

By opposition to the continuous scheme, the discontinuous scheme is not developed to ensure kinematical compatibilities between fluid mesh and structure mesh such as those given in Equation [22].

The idea is that the pressure distribution transmitted by the fluid to the structure to calculate displacements from time t_n to time t_{n+1} is taken at time t_n. Thus it introduces a discrepancy between deformed state and solicitations.

One way to get around this problem is to relax the matching condition on the fluid-structure interface. This idea may seem surprising at first since the coupling precisely carries out at this interface. But we may prove that if we ensure that the non-matching fluid and structure interfaces remain close during the calculation, the results will be more accurate and dependencies with regards to $N_{f/s}$ really weak. This scheme is inspired from works of S. Piperno essentially referenced in [PIP 94], [PIP 95a].

A complete cycle takes place as follows (Figure 11):

– The structure code determines a first estimation of the displacements solution $(\widetilde{X}^{n+1}, \widetilde{Y}^{n+1})$ at instant $(n+1)$ obtained from previous pressure data;

– This estimated structure geometry is transmitted to the fluid code i.e. displacements and velocities of all nodes respectively denoted by $(\widetilde{X}^{n+1}, \widetilde{Y}^{n+1})$ and $(\widetilde{\dot{X}}^{n+1}, \widetilde{\dot{Y}}^{n+1})$;

– Fluid variables are then advanced of $N_{f/s}$ fluid time steps in order to reach the estimated structure deformation;

– Then the fluid code transmits a pressure profile averaged on all $N_{f/s}$ time steps;

– The structure code thus calculates the corrected solution from the new pressure profile corresponding at instant $(n+1)$: (X^{n+1}, Y^{n+1});

– Back to step 1.

Concerning the boundary conditions, we will impose a constant wall velocity during the $N_{f/s}$ fluid time steps and calculated as follows:

$$\dot{X}_f^{n+1/2} = \frac{\widetilde{X}_f^{n+1} - \widetilde{X}_f^{n}}{\Delta t_s}, \qquad [25]$$

where $\widetilde{X}_f^{n+1}$ and $\widetilde{X}_f^n$ denote the estimates of fluid mesh states respectively at times (n) and $(n+1)$. This choice corresponds to the one imposed by the geometric consistency law.

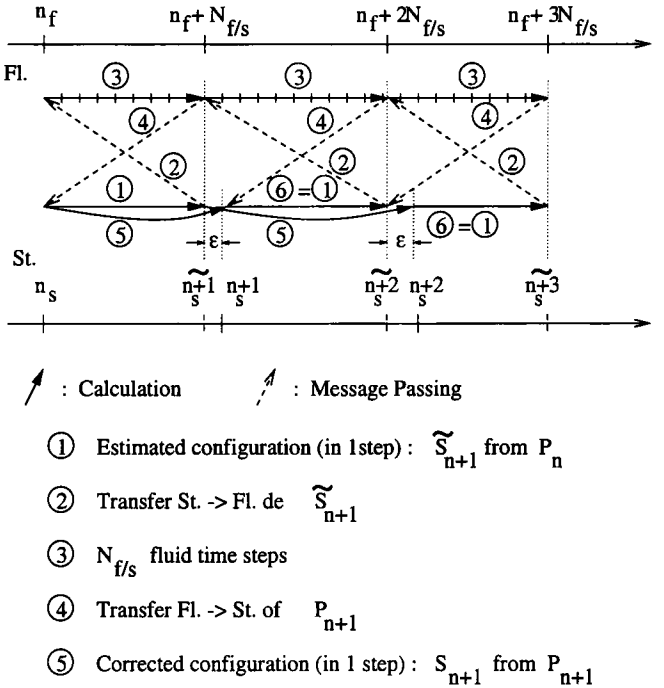

Figure 11. *Discontinuous coupling scheme*

The present scheme is more conservative than the previous one in spite of the non-compatibility between common interfaces.

Indeed, the action-reaction principle expresses as follows where the action of the structure on the fluid is still the same:

$$\text{Force (St. -> Fl.)} = \frac{\Delta t_s}{N_{f/s}} \sum_{ip=1}^{N_{f/s}} \bar{P}_{ie,ip}.$$

Concerning the force applied by the fluid on the structure, the major difference results that the pressure distribution now results from the same summation for the fluid:

$$\text{Force (Fl. -> St.)} = -\frac{\Delta t_s}{N_{f/s}} \sum_{ip=1}^{N_{f/s}} \bar{P}_{ie,ip}.$$

Thus, the conservation force principle is now exactly verified by this new scheme. We may also prove [PIP 95a] that the total energy exchange may express itself as follows:

$$E^{n+1}-E^n = \sum_{ie=1}^{nelt} \frac{L}{N_{f/s}} \left[\sum_{ip=1}^{N_{f/s}} (\bar{P}_{ie,ip} - P_{ext}) \right] \left((\epsilon_x^{n+1} - \epsilon_x^n) n_x + (\epsilon_y^{n+1} - \epsilon_y^n) n_y \right),$$

with:

$$\epsilon_x^{n+1} = X^{n+1} - \widetilde{X}^{n+1}, \quad \epsilon_x^n = X^n - \widetilde{X}^n,$$

idem for Y.

The energy variation is now a function of the difference between estimated and corrected solutions of the structure at the same time and not any longer between two successive configurations. This scheme has been validated on a *flutter* case to finally obtain similar results as well for $N_{f/s} = 5$ as for $N_{f/s} = 100$ [LEF 99a].

4. Numerical validation of the stability model

This section is dedicated to the numerical validation of the stability model by coupling two different codes, one for the structure, the other for the fluid. Precisely, we intend to validate the solicitation choice used in the model by using a numerical scheme developed with no particular consideration for this choice and recovering predicted results.

The domain considered here is the same as the one given in a previous section as well the geometry and the material properties. The fluid mesh is composed of 19750 nodes and 38827 elements (triangle of 10^{-2} m).

The structure mesh is directly extracted from the boundary of the fluid mesh to obtain conformity between both. It gives a mesh composed of 297 nodes.

Several cases have been considered for the initial position of the compression shock. This position being directly influenced by the value of the chamber pressure, positions have been obtained from 0.70 m to 2.20 m corresponding to a chamber pressure changing from 2.4 bars to 6 bars. Retained choices are shown on Figure 12 in comparison with the solution for mono-dimensional case. The wall pressure distribution resulting for many of these cases are shown on Figure 13 where the pressure jump due to the shock is well defined.

A coupling calculation, for a given chamber pressure value, is conducted along the following steps:

– A fluid calculation is conducted starting from no-flow conditions to converge to overexpanded stabilized flow. For this step, the structure is considered as rigid;

– The flexibility is given back to the structure and coupling may start. During the coupled calculation, velocity components and wall pressure are extracted every other ten nodes and stored for post-treatment. The number of fluid steps is 1.10^5;

– At the end of the calculation, all signals in displacement and pressure are treated with a Fast Fourier Transform algorithm for modal analysis.

The CFL condition for fluid stability gives a fluid time step of: $\Delta t_f = 2.7\ 10^{-6}$ s. The subcycling process is used to update the geometry configuration with $N_{f/s} = 50$.

Only linear terms of the finite element used for the structure have been retained in order to ensure consistency with the linear hypothesis of the stability model. The iterative process based on tangent matrix is however used, as for the general case of a geometrical non-linear problem.

For the coupling calculation, the objective is to test the stability of a given initial configuration.

Then, in order to consider the initial structure as an equilibrium configuration, the initial pressure distribution is extracted at the beginning of the calculation and subtracted to the current pressure profile transmitted to the structure code during each updating step.

This procedure has the advantage to avoid the determination of a deformed state in equilibrium with respect to the pressure distribution and to be exactly in accordance with the Equation [9].

We show on Table 1, the displacement and pressure spectra for several test cases indicated by the initial position of the compression shock at the bottom of each graph. The x-axis is scaled from 0 to 150 Hz.

We can make the following observations:

– The first natural peak associated to the first natural mode undergoes a significant shifting in frequency depending on the initial location of the compression shock. For the graphs from the 5^{th} to the 8^{th} columns, we do not observe single peaks any more, but a wide range of frequencies, typical of coalescing modes;

– The 2^{nd} column is related to the lowest frequency taken by the first mode, the value is around 3 Hz;

– We may also observe that peaks in frequency observed on displacement spectrum are clearly induced by pressure variation for the case where values do not correspond to any natural frequency.

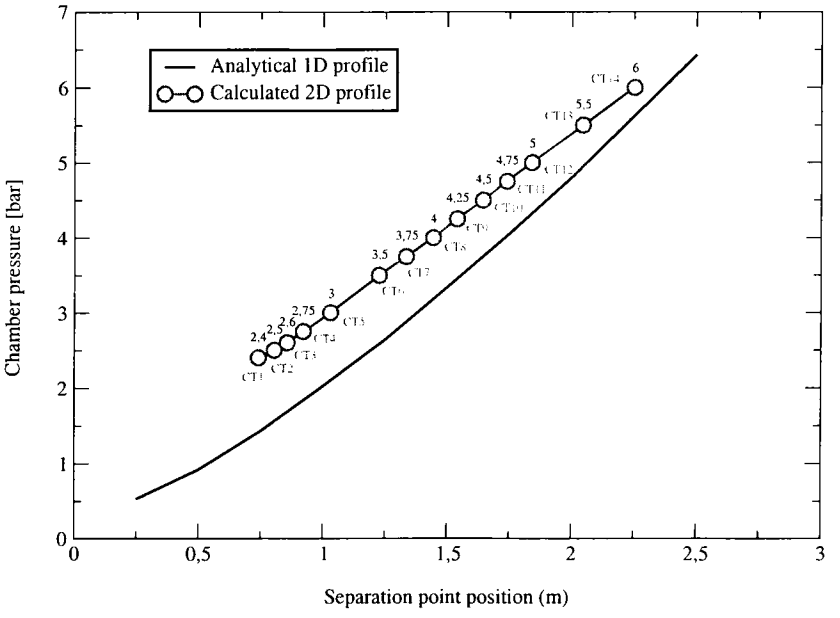

Figure 12. *Chamber pressure versus shock position*

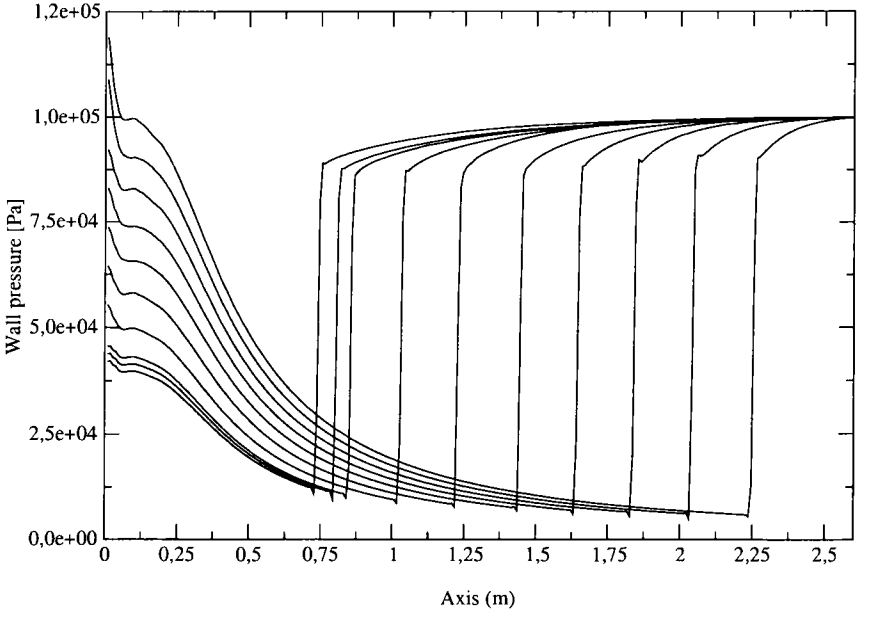

Figure 13. *Pressure parietal profiles*

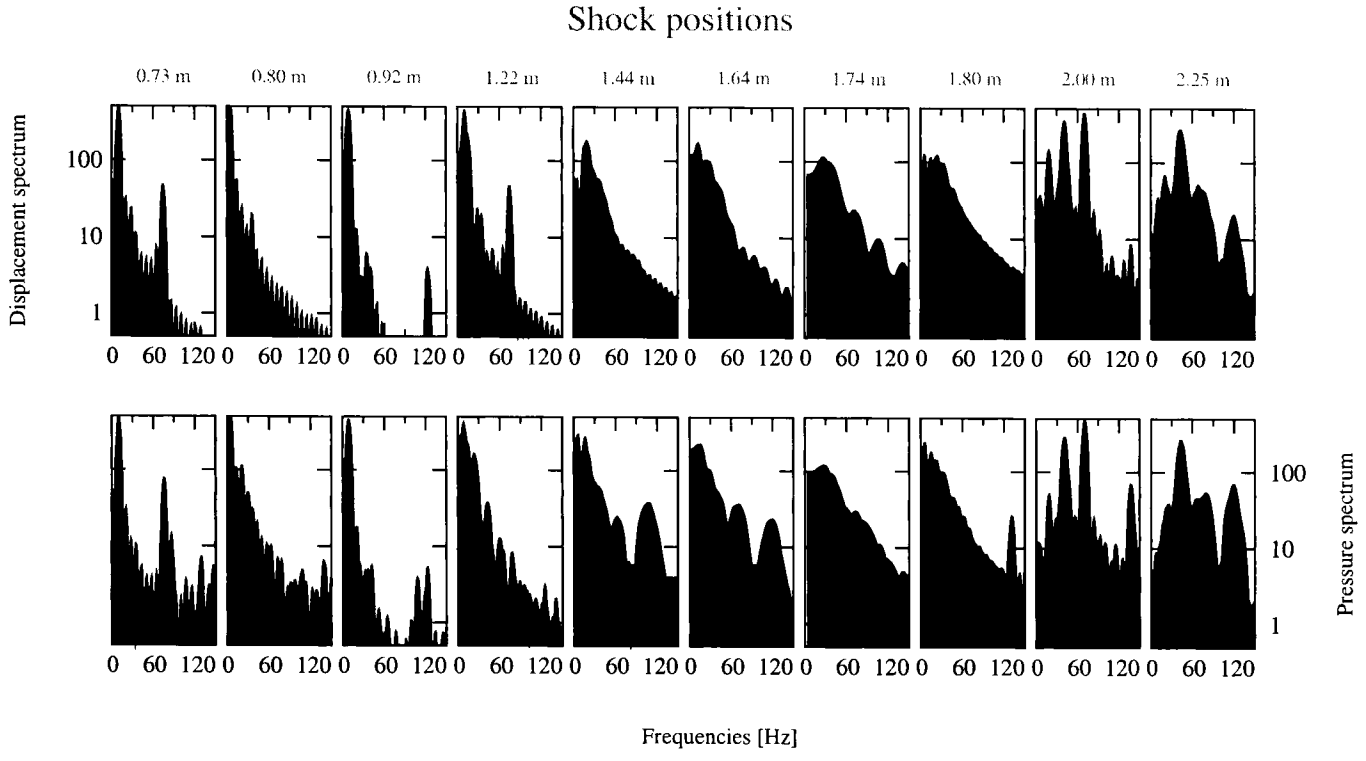

Tableau 1. *Spectrum in displacement and pressure*

For the cases corresponding to dynamical instabilities, the displacements rapidly reach order of magnitudes greater than the structure thickness. At this point, the non-linear terms become significant for the structure and must be considered. For all stable cases, displacements are of an magnitude order lower than the thickness (see Figure 14). Stable cases show higher frequencies than unstable cases essentially governed by only one coalescing frequency.

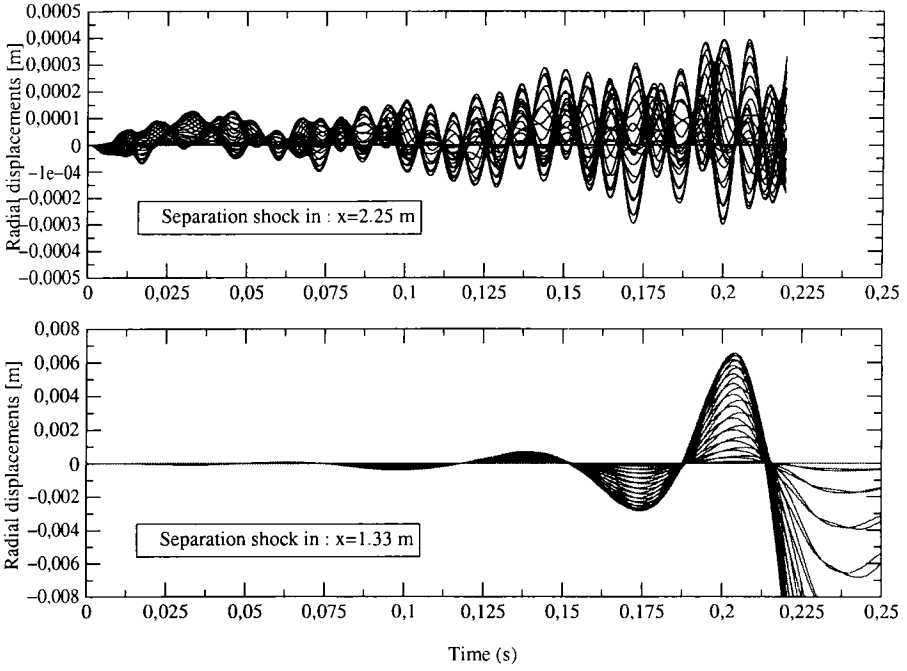

Figure 14. *Nodal displacement evolutions for stable and unstable cases*

The global set of results are shown on Figure [15] in comparison with the analytical results. We can make the following observations:

– No calculation has been conducted for a shock position lower than 0.75 m corresponding to a chamber pressure lower than 2.3 bars. Indeed for these cases, the shock never stabilizes itself and oscillates avoiding convergence of the fluid flow;

– The buckling effect has not been observed, the lowest frequency reached by the structure being about 3 Hz. This may be explained because two-dimensional effects are the most important in this region as shown with the difference of chamber profiles between mono and two-dimensional profiles, as illustrated on Figure 12. But the decrease of the first frequency is significant enough to hope that different material properties may be able to develop a numerical buckling during a coupling calculation;

– We clearly see that the first two natural frequencies tend to collapse in the region forecasted by the model. However, this range of dynamical instability seems to be wider than in the theory. For these cases, the structure undergoes an oscillating behaviour

associated to an exponential growth leading to displacements of the order of 0.20 m. It really corresponds to *flutter* phenomena;

– The frequency shift occurs essentially on the first mode and on the second one but with a smoother effect. Concerning the third and fourth modes, the shift is almost inexistent in comparison with the model. We may explain this with the accuracy of the fluid scheme that is second order at most. In the shock, we have a first order approximation to stabilize the solution. This is done in adding numerical viscosity that may be the explanation of the dissipative effects on the frequency-shift for higher modes.

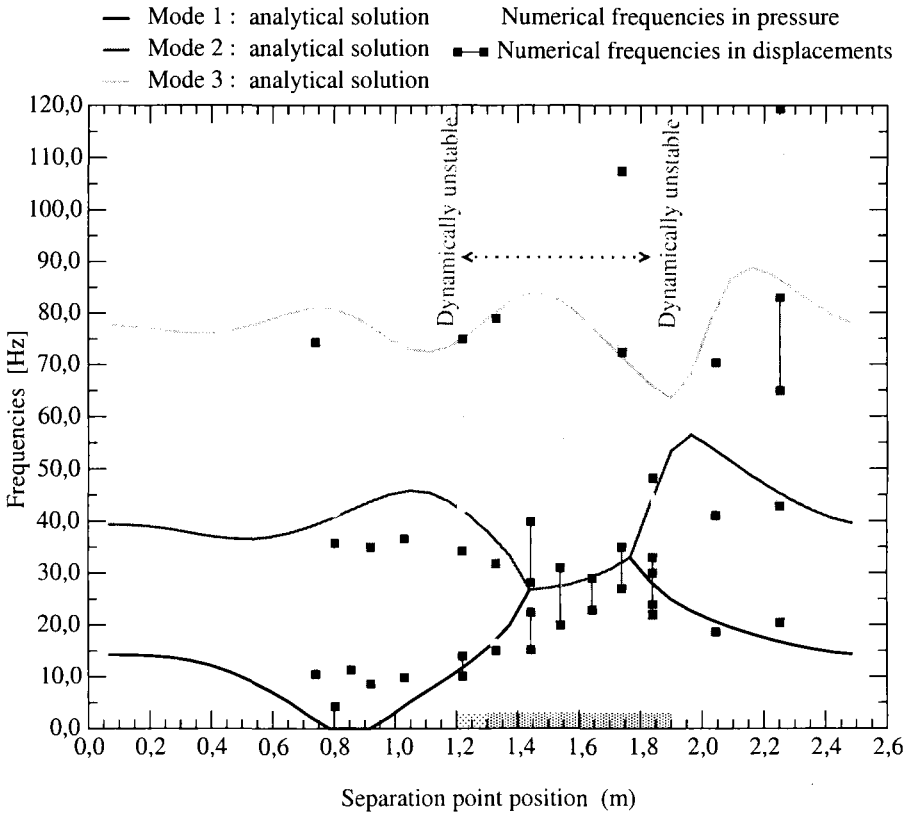

Figure 15. *Confrontation between analytical and numerical results*

On Figure 16, we display the location of the order of approximation for the fluid code. This case corresponds to an initial shock position in 1.33 m. We clearly observe the thick band of first order approximation induced by the shock capturing technique.

On the following Figures 17 and 18, we show the contours for pressure field respectively after the beginning of the coupling then at the end. The last one clearly shows the need to consider non-linear terms for taking into account large displacements. An

instability will always appear under linear assumptions but will be next controlled by non-linear terms.

On Figures 19 and 20, we represent the nodal pressure and displacement behaviours for the calculations corresponding to $x_{sep} = 1.74$ m and $x_{sep} = 2.25$ m. For each variable, the results are displayed in three graphs, respectively for nodes upstream the shock position, nodes covered by the shock displacement and nodes downstream the shock (from top to bottom).

The Figure 19 corresponds to an unstable behaviour that is confirmed with the pressure magnitude and the pressure jumps detected by the nodes swept by the shock (middle graph). The magnitude of pressure jumps is about 85000 Pa and corresponds to the ones measured on the parietal pressure profiles shown on Figure 13.

The displacement magnitude rapidly reaches large values in a very short time. Several nodes are concerned by the shock displacement that is important, since signals are extracted each ten nodes, the distance between each signal-point being of 0.1 meter. We may observe correlations between pressure and displacements for nodes upstream the shock, corresponding to supersonic flow. Both signals clearly adopt the same sinusoidal form. We also observe a discrepancy between pressure and displacement with a backwardness for the pressure that may be responsible of the exponential growth after each cycle of oscillation.

Concerning the Figure 20, the magnitude for both pressures and displacements signals are of an order compatible with a linear stable behaviour. This time, only one node is attached to the shock displacement. This means that the shock remains located in a narrow area. We still observe the same correlations between pressure and displacements for the upstream nodes.

Now, there are figures concerning the computing times: The calculations have been conducted on two kind of computers. The CPU time dedicated to structure dynamics is about 1% for any coupled calculations. Main results are shown on the following table:

Computer type	Iterations	CPU for fluid	CPU for structure	Total CPU
Pentium III 550	10000	453'	6'	459'
		98.7 %	1.3 %	—
SGI R 10000 195	10000	512'	5'	517'
		98.95 %	1.05 %	—

Table 2. *CPU time shared between both codes*

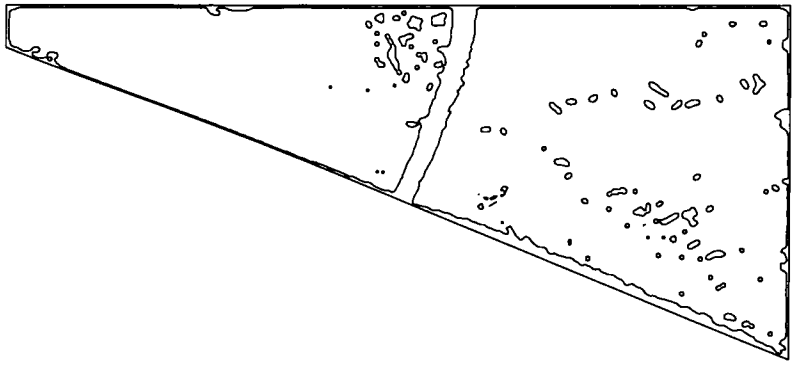

Figure 16. *Spatial location of precision order*

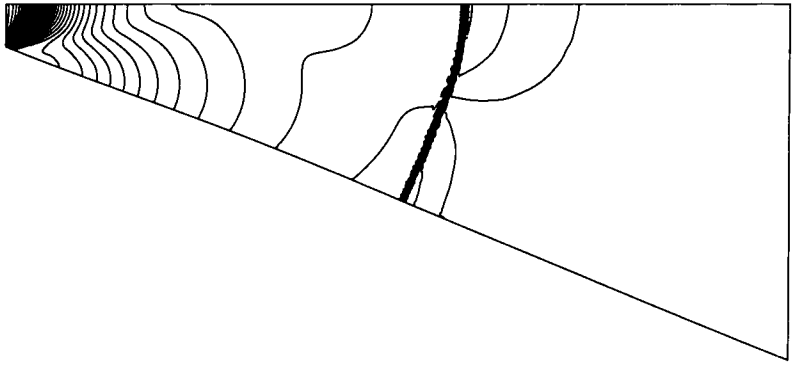

Figure 17. *Pressure contours at the beginning, min.: 0.059 bar, max.: 2.113 bar*

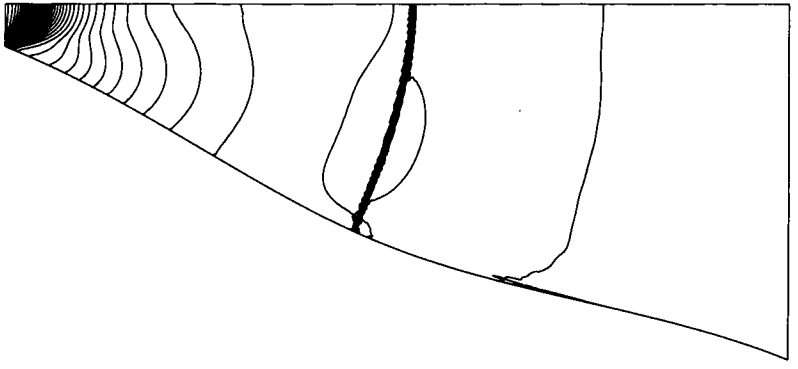

Figure 18. *Pressure contours at the end, min.: 0.052 bar, max.: 2.113 bar*

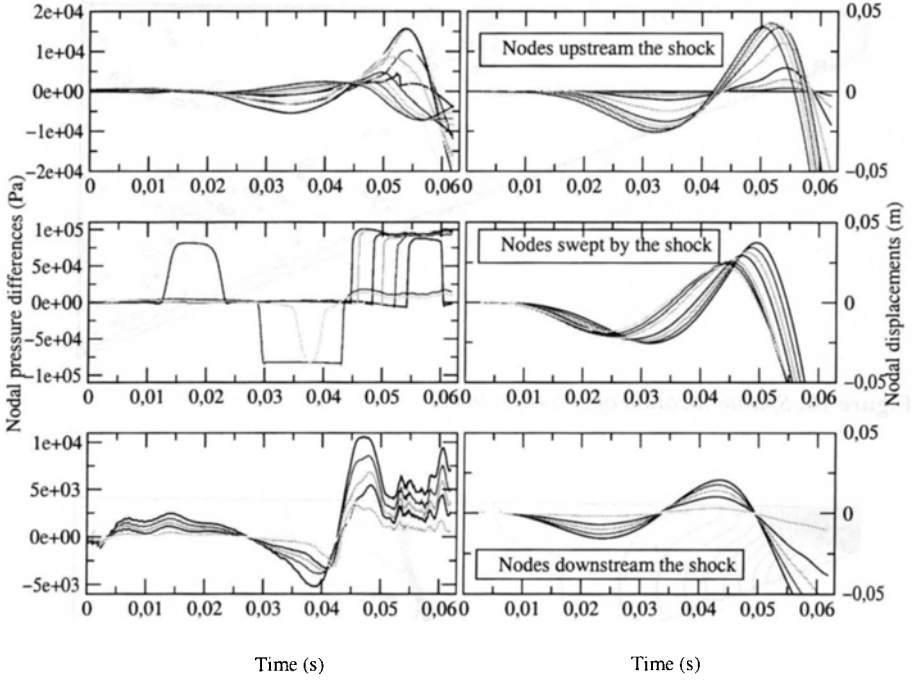

Figure 19. *Pressure-displacements correlation for the case:* $x_{sep} = 1.74\ m$

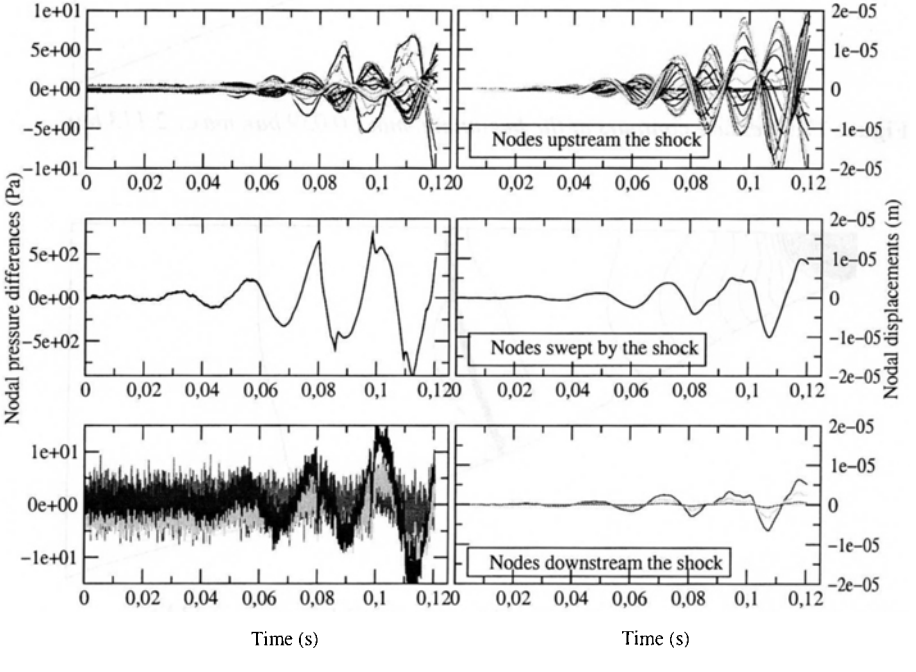

Figure 20. *Pressure-displacements correlation for the case:* $x_{sep} = 2.25\ m$

The gain with the Pentium is about 20% but could be improved in using a Fortran version with better compilation options.

5. Conclusion

In this paper, a stability model for aeroelastic behaviour on an overexpanded flexible nozzle has been developed based on an improvement of Pekkari's model [PEK 93]. The main difference between both models concerns the choice of the projection base used for modal superposition analysis. These models are both based on a solicitation expression issued from the linear piston approximation.

The objective was to study the influence of the separation shock position on all the natural vibration modes. The model developed here is able to take into account dynamical instabilities and is consistent with Pekkari's model that is only able to detect static ones. An analytical validation was then conducted with a particular material properties choice that confirmed, for the retained solicitation form, the existence of both static and dynamic instabilities.

In a second part, a numerical model for fluid-structure interaction was then exposed with the description of two codes, one dedicated to structure, the other one for the fluid. A discussion followed on the choice of the coupling scheme to use. We have shown that the non-satisfaction of kinematic compatibility was the better way to ensure energy and momentum conservations [PIP 95a].

In a third part, the same previous validation case was then conducted with the coupling model to verify the correct choice of solicitation form introduced in the stability models. We thus observed that the structure undergoes a *flutter* effect for initial shock position in accordance with the stability model. However, the buckling effect has not been observed for reasons that seem essentially related to two-dimensional effects. They seem to introduce significant differences between analytical and calculated frequency evolution. But we observe all the same a first natural mode going down to 3 Hz.

Both models of stability are consistent even if Pekkari's one is not dedicated to detect dynamical behaviours in the sense where two frequencies may collapse. But for three-dimensional analysis, this model is cheaper in computation cost because natural modes have to be determined only one time, whereas, for each new shock position, the developed model of this paper has to conduct new modal analysis at each time.

We also observed that frequency shift effect essentially acts on the first two natural modes only, due to the dissipative effect of shock capturing and only second order for fluid scheme. Next works will consist in using a WENO scheme [LIU 94] for the fluid code in order to avoid the excessive dissipation of the FCT technique and to globally improve the precision order up to five. The aim will be to increase the accuracy in the numerical frequency shift and detect effects on higher modes.

In conclusion, this work seems to confirm the dynamical coupling of a flexible nozzle with regards to overexpanded flows. Even if experimental data are quasi-inexistent, the astronautic industries express a growing interest in such a numerical study that seems promising to offer a better understanding of the coupling physics underlying aeroelasticity on rocket engines.

These works have been partly realized with the support of computer resources (CRIHAN - Centre de Ressources Informatiques de Haute-Normandie) financed as part of article 12 of the CPIPB - Inter-regional pole of modeling for engineering sciences.

The first author is currently supported and financed by CNES (Centre National d'Études Spatiales) for a post-doctoral position under the contract No 99/CNES/5652 for studying aeroelasticity on flexible nozzle. This work is associated to a research group between CNES/ONERA/CNRS/SNECMA/Aérospatiale-Matra on jet flows in nozzle and after bodies of rocket launchers.

6. References

[AMM 96] AMMAR S., « Résolution des problèmes non linéaires », PhD thesis, Département Génie Mécanique, Université Laval, Québec, 1996.

[ASH 56] ASHLEY H., ZARTARIAN G., « Piston Theory - A New Aerodynamic Tool for the Aeroelastician », *Journal of the Aeronautical Sciences, pp.1109-1118*, 1956.

[BIS 75] BISPLINGHOFF R. L., ASHLEY H., *Principles of Aeroelasticity*, Wiley and Son, New York, 1975.

[BOR 97] BORIS J. P., BOOK D. L., « Flux-Corrected Transport, I. SHASTA, a Fluid Transport Algorithm That Works », *Journal of Comp. Physics, 135, pp.172-186, (original publication : 1973)*, 1997.

[BOU 93] BOULERHCHA M., « Ecoulements Eulériens par Eléments Finis avec Raffinement de Maillage; comparaison d'un schéma centré et de schémas décentrés », PhD thesis, Département de Génie Mécanique, Faculté des Sciences et de Génie, Université Laval, Québec, 1993.

[CAN 90] CANDEL S., *Mécanique des Fluides*, Dunod Université, 1990.

[COR 92] CORMACK R. W. M., « Numerical Computation of Compressible Viscous Flow », Stanford University course, February 1992.

[DHA 95a] DHATT G., FAFARD M., « Mécanique non linéaire », rapport, Septembre 1995, Institut pour la Promotion des Sciences de l'Ingénieur - Paris.

[DHA 95b] DHATT G., FAFARD M., « Modélisation des coques en grandes rotations », rapport, Septembre 1995, Institut pour la Promotion des Sciences de l'Ingénieur - Paris.

[DHA 95c] DHATT G., FAFARD M., « Résolution de problèmes non linéaires », rapport, Septembre 1995, Institut pour la Promotion des Sciences de l'Ingénieur - Paris.

[DOW 75] DOWELL E. H., *Aeroelasticity of Plates and Shells*, Noordhoff International Publishing, 1975.

[FAR 96] FARHAT C., « High Performance Simulation of Coupled Non-linear Transient Aeroelastic Problems », *Ecole d'Eté - Porquerolles (France) 1-6 Juillet*, 1996.

[FOR 49] FORSTER C., COWLES F., « Experimental Study of Gas Flow Separation in Overexpanded Exhaust Nozzles for Rocket Motors », rapport n° No. 4-103, 1949, JPL-Progress.

[FUN 58] FUNG Y. C., *An Introduction to the Theory of Aeroelasticity*, Wiley and Son, New York, 1958.

[GEI 94] GEIST A., BEGUELIN A., AL., « PVM 3 User's Guide and Reference Manual », rapport, May 1994, Oak Ridge National Laboratory.

[HAD 97] HADJADJ A., « Analyse Physique et Simulation Numérique des Ecoulements Compressibles; Application aux Tuyères de Propulseurs », PhD thesis, LMFN-CORIA, Université Rouen - France, 1997.

[KES 97] KESSY E., « Décomposition de domaine et calcul parallèle distribué: Application à la mécanique des fluides », PhD thesis, LMFN-CORIA, Université Rouen - France, 1997.

[KON 87] KONDO N., TOSAKA N., AL., « Numerical Simulation for Coupled System of Viscous Flow and Elastic Shell », *Numerical Methods in Laminar and Turbulent Flow, Vol. 4, Part 2, p 1798*, 1987.

[LAX 60] LAX P. D., WENDROFF B., « Systems of Conservation Laws », *Comm. Pure and Applied Mathematics, 13 : pp. 217-237*, 1960.

[LEB 94] LEBAIL F., POPP M., « Engineering Aspects of Side Load Prediction », rapport, novembre 1994, WP-1 Study Note, Phase 2, Deutsche Aerospace, ESTEC-ELITE Advanced Nozzle Aerodynamics.

[LEF 98] LEFRANÇOIS E., « Modèle numérique de Couplage Fluide-Structure pour l'Etude des Phénomènes Aéroelastiques avec Application aux Moteurs Fusée », PhD thesis, LMFN-CORIA, Université de Rouen, Juin 1998.

[LEF 99a] LEFRANÇOIS E., « Étude numérique du phénomène de charges latérales au sein des moteurs fusée avec aéroélasticité », Rapport de recherche, convention n^o 99/cnes/5652, 1999, CNES.

[LEF 99b] LEFRANÇOIS E., DHATT G., VANDROMME D., « Fluid-Structural Interactions with Applications to Rocket Engines », *International Journal for Numerical Methods in Fluids,Vol. 30 - 1999, pp. 865-895*, 1999.

[LEF 99c] LEFRANÇOIS E., DHATT G., VANDROMME D., « Modèle numérique de couplage fluide-structure avec applications aux moteurs fusée », *Revue européenne des éléments finis, Vol. 8 - No 2/1999, pp. 159-199*, 1999.

[LIU 94] LIU X., OSHER. S., CHAN T., « Weighted Essentially Non-Oscillatory Schemes », *J. Comput. Phys.*, vol. 115, 1994, p. 200-212.

[NAV 73] NAVE L. H., COFFEY G. A., « Sea Level Side Loads in High-Area-Ratio Rocket Engines », *AIAA Paper, No. 73-1284*, 1973.

[PAR 85] PARROT A. K., CHRISTIE M. A., « FCT Applied to the 2-D Finite Element Solution of a Tracer Transport by a Single Phase Flow in a Porious medium », *ICFD Conf. on Numerical Methods in Fluid Dynamics, Reading*, 1985.

[PEK 93] PEKKARI L. O., « Aeroelastic Stability of Supersonic Nozzles with Separated Flow », *AIAA, 29th Joint Propulsion Conference and Exhibit, Monterey, CA*, 1993.

[PIP 94] PIPERNO S., « Staggered Time Integration Methods for a One-Dimensional Euler Aeroelastic Problem », rapport, Décembre 1994, CERMICS, INRIA - Sophia-Antipolis, France.

[PIP 95a] PIPERNO S., « Simulation Numérique de Phénomènes d'Interaction Fluide Structure », PhD thesis, Ecole Nationale des Ponts et Chaussées, june 1995.

[PIP 95b] PIPERNO S., FARHAT C., LARROUTUROU B., « Partitioned Procedures for the Transient Solution of Coupled Aeroelastic Problems. Part I: Model Problem, Theory and Two-Dimensional Application », *Comput. Methods Appl. Mech. Engrg. 124, pp. 79-112*, 1995.

[Pro98] Proceedings, CNES PARIS, *European Seminar on Rocket Nozzle Flows*, October 1998.

[REE 95] REED D., HIDALGO J., « Fluctuating Pressure Analysis of a 2-D SSME Nozzle Air Flow Test », *Workshop for Computational Fluid Dynamic Applications in Rocket Propulsion and Launch Vehicle Technology - Huntsville, Alabama*, 1995.

[ROM 98] ROMINE G. L., « Nozzle Flow Separation », *AIAA Journal, No. 9*, 1998.

[SCH 73] SCHMUCKER R. H., « Side Loads and their Reduction in Liquid Rocket Engines », rapport, October 1973, 24th Int. Astron. Congress, Baku, USSR.

[SCH 84] SCHMUCKER R. H., « Flow Processes in Overexpanded Chemical Rocket Nozzles - Part I », rapport, 1984, NASA Report - 77396.

[SER 96] SERAM-CNES, « Etude du Comportement Dynamique du Divergent du Moteur VULCAIN », rapport, 1996, Laboratoire de Mécanique des Structures secteur ENSAM, Université Paris VI - Dossier 60737.

[SUM 54] SUMMERFIELD M., FOSTER C., SWAN W., « Flow Separation in Overexpanded Supersonic Exhaust Nozzles », *Jet Propulsion*, vol. 24, n° 9, 1954, p. 319-320.

[TAL 96] TALLEC P. L., MOURO J., « Structures en grands déplacements couplées à des fluides en mouvement », rapport, August 1996, INRIA - *n°* 2961.

[TUO 68] TUOVILA W. J., LAND N. S., « Experimental Study of Aeroelastic Instability of Overexpanded Rocket Nozzle Extensions », rapport, April 1968, NASA TN D-4471.